sequence of reflection symmetry breaking in the d_{z^2} orbital, due to the (axial) histidine ligation, rather than as a result of the changes in iron out-of-plane displacement that occur as the system relaxes. However, as discussed by A. M. Ahmed *et al.* [*Chem. Phys.* **158**, 329 (1991)], the frequency of the Fe–His mode may well be affected by structural changes associated with the protein relaxation process.
14. The available evidence from x-ray crystallography of model compounds [W. R. Scheidt and P. Piciulo, *J. Am. Chem. Soc.* **98**, 1913 (1976)] suggests that the Fe–His bond is extended in the NO bound state, relative to the unbound species, as a result of additional electron density in the antibonding d_{z^2} orbital.
15. The factor of π arises under the condition $\tau_c \ll \tau_p$ because τ_p (~75 fs) corresponds to one-half of the Fe–His oscillatory period (~150 fs). A much smaller phase shift is expected for the low-frequency doming mode because τ_p is a much smaller fraction of its oscillatory period. The bound on τ_c ($\ll$75 fs) is somewhat shorter than (but not inconsistent with) that in previous studies, where the time scale for photodissociation was given as <50 fs [J. Petrich, C. Poyart, J. L. Martin, *Biochemistry* **27**, 4049 (1988)], with the heme undergoing a major fraction of its initial out-of-plane displacement within the first 30 to 50 fs of photolysis [J. Petrich *et al.*, *ibid.* **30**, 3975 (1991)].
16. M. Walters and T. G. Spiro, *Biochemistry* **21**, 6989 (1982).
17. F. W. Wise, M. Rosker, G. Millhauser, C. L. Tang, *IEEE J. Quantum Electron.* **QE-23**, 1116 (1987).
18. X. Y. Li and M. Zgierski, *Chem. Phys. Lett.* **188**, 16 (1992).
19. Supported by National Science Foundation grant 94-05979 and National Institutes of Health grant AM-35090. We thank G. Millhauser for supplying us with the LPSVD algorithm and L. D. Ziegler for numerous helpful conversations.

24 June 1994; accepted 9 September 1994

Simulations of Atmospheric Variability Induced by Sea Surface Temperatures and Implications for Global Warming

Arun Kumar,* Ants Leetmaa, Ming Ji

An atmospheric general circulation model was forced with observed interannual changes in the global sea surface temperatures (SSTs) for the period 1982 to 1993. The simulated seasonal surface air temperature patterns over land areas closely resemble the observed. Over most of the globe, the patterns also resemble those associated with El Niño events and are also reproduced in simulations with weak warm tropical SSTs near the date line. An exception is northern Asia, where the mechanisms for the observed warming are unclear. The results suggest that enhanced air-sea interactions resulting from recent, more persistent warm oceanic conditions in the tropics contributed to the observed global warming trend during this period.

Dominant interannual changes in the SST in the tropical Pacific Ocean are related to the quasi–periodic evolution of El Niño phenomena. These changes can have appreciable impact on the tropical and mid-latitude atmospheric temperatures (*1*). Although the impact of tropical SSTs on the tropical atmosphere has long been well simulated in atmospheric general circulation models (AGCMs) (*2, 3*), the impact on the mid-latitude atmospheric flows is only beginning to be realized (*4, 5*). Recent advances in the AGCMs have reached a stage where the impact of tropical SSTs on the global atmospheric flows can now be simulated.

To assess the capability of the National Meteorological Center (NMC) climate AGCM for seasonal prediction, we carried out several extended-range integrations forced with observed SSTs. This AGCM has a spectral triangular truncation at horizontal wave number 40 (T40) and has 18 levels in the vertical direction. The grid resolution of T40 is about 3° in latitude and longitude. It is a lower resolution and differently tuned version of the AGCM used routinely at NMC for global short-range weather forecasts (*6*). We consider four model integrations. Integration (i) is 20-year integration with a climatological annual cycle of SSTs; the SSTs are an average of those observed for the period 1950 to 1980 (*7*). The atmospheric statistics resulting from this integration serve as the reference state from which anomalies in the other integrations are calculated. Model (ii) combines nine integrations all starting from 1 February 1982 with slightly different initial conditions and extending to 31 December 1993 in which the observed global SSTs (*7*) serve as the boundary conditions. Multiple runs are necessary to minimize the influence of atmospheric internal variability, which for a single run, can dominate the SST influence. Integration (iii) is a 20-year integration in which the global SST anomaly for the month of January 1992 was superimposed on the climatological annual cycle of SST used in (i). This represents conditions at the height of an El Niño. Integration (iv) is a 10-year integration similar to case (iii) but with SST anomalies as the mean of those for January, February, and March 1991 reduced in amplitude by a factor of 2. This represents a weak tropical warming in the vicinity of the date line similar to that generally preceding a mature warm event.

All other boundary conditions—for example, ground wetness and snow depth—were treated as prognostic variables. All integrations used a CO_2 content of 330 parts per million. The monthly mean statistics for all the runs were generated by averaging the respective month over all years of integration. For example, the January mean for (i) would be the mean of 20 Januarys resulting from 20 years of integration.

The observed temperature anomalies averaged from December to May for the years 1982 to 1992 show regions of warming located over North America, Africa, Australia, northern Europe, and Asia (Fig. 1A) (*8*). Regions of cooling are located over Greenland, Mexico and the southwestern United States, northern India, and southeast Asia. The winter and spring period were chosen for the averaging because this was the period that shows warming as documented in the Intergovernmental Panel on Climate Change (IPCC) report (*9*). Globally, the AGCM–generated response in integration (ii) (Fig. 1B) closely resembles the observed anomalies. Although the match is not perfect, the comparison implies that the observed continental air temperature anomalies result from anomalous air-sea interactions because the only externally specified forcing in this simulation was the SSTs.

The main interannual climate variation associated with air-sea interactions is the El Niño–Southern Oscillation (ENSO) phenomenon. It is thus relevant to ask whether the observed global air temperature anomalies (Fig. 1A) are in response to this. To estimate the ENSO-related signal, we composited the observed air temperatures for those years between 1950 and 1993 when either major warm or cold events occurred. This period included a total of 18 events, nine of each sign. The air temperature anomalies for the cold ENSOs were almost everywhere of the opposite sign than those for the warm ENSOs. The structure of the composite anomaly, the average for the warm minus the cold ENSOs (Fig. 1C), is almost everywhere identical to that of Fig. 1A. The main discrepancies are the region around and poleward of 60°N in central Asia—where in contrast to Fig. 1A, the El Niño composite shows anomalies of opposite sign—and the northeast region of North America, which is not as cold. A similar compositing for integration (ii) indicates that the model response resembles the observed composite in Fig. 1C except (i) it is too strong in the tropical eastern hemisphere (*10*) and (ii), poleward of 70°N, it has temperatures that are too high. The anomaly

National Meteorological Center, 5200 Auth Road, Camp Springs, MD 20746, USA.

*To whom correspondence should be addressed.

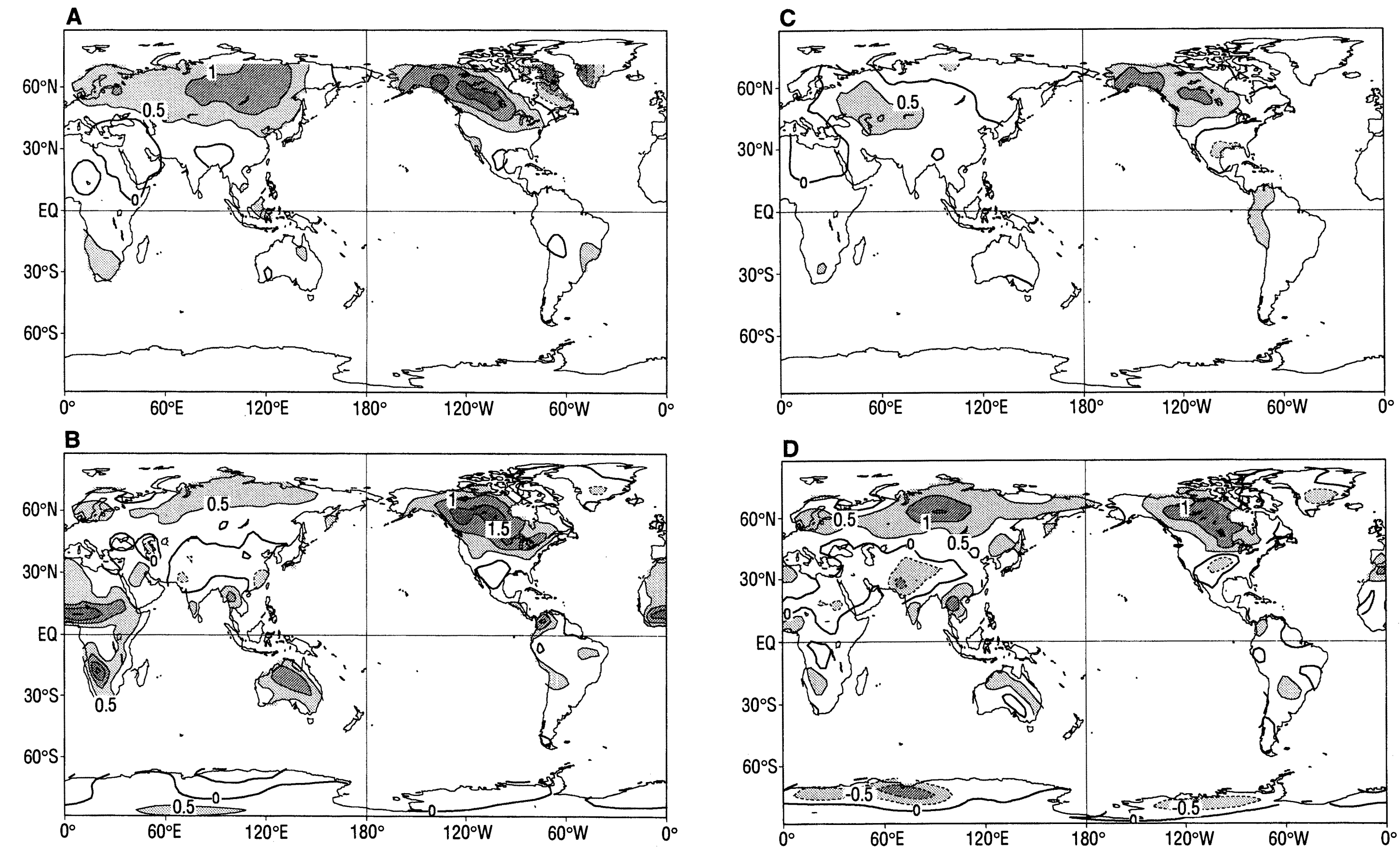

Fig. 1. (**A**) Geographical distribution of observed surface air temperature anomalies (in kelvin) for the period 1980 to 1993 relative to 1950 to 1980. (**B**) Surface air temperature anomalies for the AGCM forced with the observed SSTs of 1982 to 1993 relative to the climatological SST integration. (**C**) Surface temperature anomaly for ENSO composite relative to 1950 to 1980. The nine warm events are 1958, 1966, 1970, 1973, 1977, 1978, 1983, 1987, and 1992, and the nine cold events are 1950, 1951, 1955, 1956, 1971, 1974, 1976, 1985, and 1989. (**D**) Same as (B) but for AGCM integration with the mean of January, February, and March 1991 SSTs reduced uniformly in amplitude by a factor of 2 and superimposed on the climatological seasonal cycle. The anomalies are averages for December to March. The contour interval is 0.5 K.

pattern for integration (iv) (Fig. 1D) with weak warming at the date line also is quite similar to that in Fig. 1C and implies that a major ocean warming in the eastern Pacific is not required to produce an atmospheric response similar to one triggered by a major El Niño.

The IPCC report also indicates that the observed warming in the recent decade was confined to the winter and spring seasons. During the fall, a cooling was observed (9). A compositing of the observations (similar to that in Fig. 1C) shows the same to be true for the observed ENSO response. Similar results are obtained in integration (iii) (Fig. 2). The remote atmospheric response in mid-latitudes results from the teleconnection response to the tropical heating anomalies forced by the tropical SST anomalies (*11*), and this remote response is sensitive to the atmospheric mean state (*12, 13*). Thus, the mid-latitude impact of a fixed tropical ENSO SST anomaly of one sign depends on the season (Fig. 2).

Global surface air temperatures since 1981 have markedly changed with a strong seasonal and regional dependence (9). These changes are very similar to the observed response of an ENSO composite (Fig. 1, A and C). The AGCM results, both for the strong ENSOs and weak warming in the vicinity of the date line, also have a global response similar to the observed ENSO composite. Since 1981, three major El Niños, as well as a persistent warming near the date line from 1990 onward, have occurred. However, only one major and one smaller cold event took place during this period. Hence, events in the tropics during this period were biased toward the production of the spatial and seasonal pattern of continental air temperature anomalies that would resemble the response of the ENSO composite. If the tropical SST warm bias was a consequence of natural variability, then most of the observed warming trend during this period could be explained as the natural variability of the ocean-atmosphere system on the decadal or longer time scale (*14*). The regions where this does not appear to be the case are northern Asia and the region surrounding Greenland where the trends could not be explained in terms of an ENSO-related signal

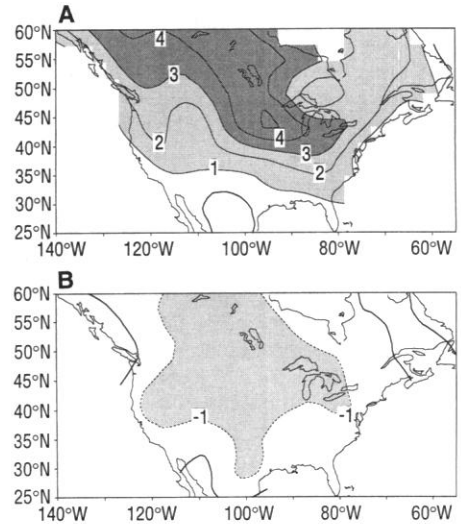

Fig. 2. Seasonal dependence of the surface air temperatures anomalies (in kelvin) for AGCM integration with January 1992 SST anomaly superimposed on the climatological seasonal cycle. Anomalies are averages for (**A**) January and February and (**B**) October. The contour interval is 1.0 K.

alone. However, all of the model simulations, which used global SST anomalies, did produce these (Fig. 1, B and D). It is likely that the model responses in these regions are the result of extratropical anomalies. Results from a subsequent suite of numerical experiments performed to separate the effects of various tropical and extratropical SST anomalies also suggest this connection.

This investigation does not preclude the possibility that the observed warming of the tropical oceans is the end result of global warming itself. If so, our results imply that the spatial and temporal characteristics of the global warming trends are manifested as a bias in the frequency of occurrence of one of the modes of the natural variability of the ocean-atmosphere system, that is, ENSO. As a corollary, the AGCMs that do not simulate these modes of natural variability for the present climate may also misrepresent the spatial and temporal characteristics of predicted global warming.

REFERENCES AND NOTES

1. M. S. Halpert and C. H. Ropelewski, *J. Clim.* **5**, 577 (1992).
2. M. L. Blackmon, J. E. Geisler, E. J. Pitcher, *J. Atmos. Sci.* **40**, 1410 (1983).
3. N. C. Lau, *Mon. Weather Rev.* **113**, 1970 (1985).
4. L. Bengtsson *et al.*, *Science* **261**, 1026 (1993).
5. M. Ji, A. Kumar, A. Leetmaa, *Tellus A* **46**, 398 (1994).
6. M. Kanamitsu, *Weather Forecast.* **4**, 335 (1989).
7. R. W. Reynolds, *J. Clim.* **1**, 75 (1988).
8. For the source of observed surface temperature-data, see C. F. Ropelewski, J. E. Janowiak, M. S. Halpert, *Mon. Weather Rev.* **113**, 1101 (1985).
9. J. T. Houghton, B. A. Callander, S. K. Varney, Eds., *Climate Change: The Supplementary Report to the IPCC Scientific Assessment* (Cambridge Univ. Press, Cambridge, 1992).
10. The model error for the ENSO composite in the tropical eastern hemisphere can also be seen in the comparison of Fig. 1, A and B.
11. J. D. Horel and J. M. Wallace, *Mon. Weather Rev.* **109**, 813 (1981).
12. M. P. Hoerling *et al.*, *J. Clim.* **5**, 669 (1992).
13. J. D. Opsteegh and H. M. Van den Dool, *J. Atmos. Sci.* **37**, 2169 (1980).
14. Conclusions similar to this have been obtained in an observational study by K. E. Trenberth and J. W. Hurrell [*Clim. Dyn.* **9**, 303 (1994)].

15. Support provided by National Oceanic and Atmospheric Administration's office of Global Programs through the Climate and Global Change Program is gratefully acknowledged.

23 May 1994; accepted 7 September 1994

Causes of Decadal Climate Variability over the North Pacific and North America

M. Latif* and T. P. Barnett

The cause of decadal climate variability over the North Pacific Ocean and North America is investigated by the analysis of data from a multidecadal integration with a state-of-the-art coupled ocean-atmosphere model and observations. About one-third of the low-frequency climate variability in the region of interest can be attributed to a cycle involving unstable air-sea interactions between the subtropical gyre circulation in the North Pacific and the Aleutian low-pressure system. The existence of this cycle provides a basis for long-range climate forecasting over the western United States at decadal time scales.

The origins of decadal climate variability over the North Pacific Ocean and North America, characterized by anomalous surface temperatures and surface pressures (*1–4*), are uncertain. A recent example of the impact of such decadal climate variability is the multiyear drought over the southwestern United States. It has been speculated by some researchers that unstable air-sea interactions over the North Pacific and changes in the large-scale ocean circulation might force the decadal climate variability (*5, 6*), while other studies suggest that tropical forcing is a stronger influence (*2, 4, 7*). In this report, we develop a consistent physical picture of how decadal climate variability over the North Pacific and North America may be generated.

To study the decadal climate variability, we used a state-of-the-art coupled model of global ocean-atmosphere general circulation (ECHO) (*8*), which was forced by seasonally varying insolation and integrating for 70 years. The coupled model simulates well the mean climate and observed short-term interannual variability. In particular, it simulates realistically the El Niño–Southern Oscillation (ENSO) phenomenon. An earlier version of this model was also applied successfully to predict the behavior of ENSO (*9*). The coupled model simulates pronounced decadal variability over the North Pacific and North America during the course of the 70-year integration. One example (Fig. 1A) of such variability is the anomalous sea surface temperature (SST) in the western Pacific in the region of the Kuroshio extension. Simulated SSTs in this region exhibit a distinct irregular oscillatory behavior on a decadal time scale with maximum anomalies of slightly less than 1°C. There are three manifestations of the decadal mode.

To determine the spatial coherence of the decadal-scale SST variability, we computed the associated SST regression pattern (Fig. 1B). It is dominated by a large-scale positive SST anomaly centered near 35°N and extending from the Asian coast almost across the entire Pacific. The orientation of this positive anomaly coincides approximately with the position of the model Kuroshio current and its eastward extension. The positive SST anomaly is surrounded by negative anomalies, most prominently in the south. The space-time structure of the SST anomalies can be represented as a combination of a standing wave pattern and a propagating pattern, with the latter component dominating in the region of the Kuroshio and its extension. The spatial structure of the SST anomalies affects the meridional temperature gradient in the Pacific, which has important consequences for

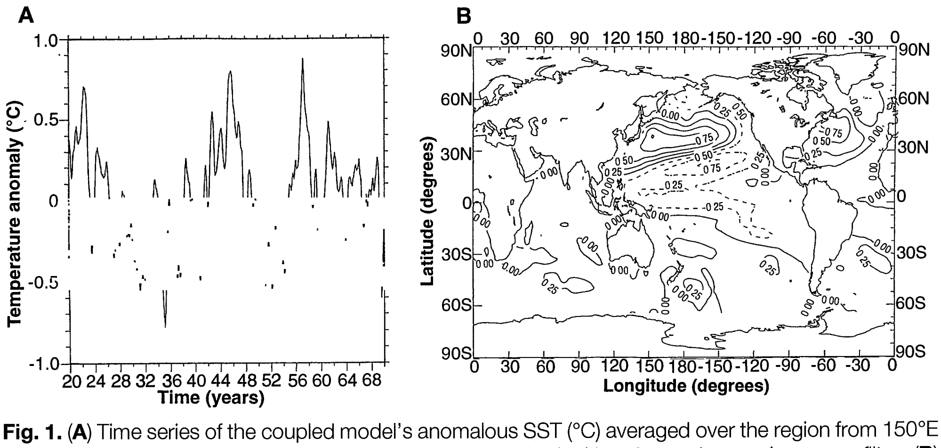

Fig. 1. (**A**) Time series of the coupled model's anomalous SST (°C) averaged over the region from 150°E to 180°E and 25°N to 35°N. The time series was smoothed with a 9-months running mean filter. (**B**) Spatial distribution of linear regression coefficients between the index time series shown in (A) and SST values. The pattern was scaled so that the maximum SST anomalies were to 1°C.

M. Latif, Max-Planck-Institut für Meteorologie, Bundesstrasse 55, D-20146 Hamburg, Germany.
T. P. Barnett, Climate Research Division, Scripps Institution of Oceanography, La Jolla, CA 92093–0224, USA.

*To whom correspondence should be addressed.